SLAC–PUB–8783

February 2001

Operation of the Cherenkov Detector DIRC of BABAR at High Luminosity *

I. Adam,[1] R. Aleksan,[2] D. Aston,[1] M. Benkebil,[4] D. Bernard,[5] G. Bonneaud,[5] F. Brochard,[5] D.N. Brown,[6] P. Bourgeois,[2] J. Chauveau,[3] J. Cohen-Tanugi,[5] M. Convery,[1] G. de Domenico,[2] A. de Lesquen,[2] S. Emery,[2] S. Ferrag,[5] A. Gaidot,[2] T. Geld,[9] G. Hamel de Monchenault,[2] C. Hast,[4] A. Hoecker,[4] R.W. Kadel,[6] J. Kadyk,[6] M. Krishnamurthy,[8] H. Lacker,[4] G.W. London,[2] A. Lu,[7] A.-M. Lutz,[4] G. Lynch,[6] G. Mancinelli,[9] F. Martinez-Vidal,[3] N. Mayer,[2] B.T. Meadows,[9] D. Muller,[1] S. Plaszczynski,[4] M. Pripstein,[6] B.N. Ratcliff,[1] L. Roos,[3] E. Roussot,[5] M.-H. Schune,[4] J. Schwiening,[1] V. Shelkov,[6] M.D. Sokoloff,[9] S. Spanier,[1] J. Stark,[3] A.V. Telnov,[6] Ch. Thiebaux,[5] G. Vasileiadis,[5] G. Vasseur,[2] J. Va'vra,[1] M. Verderi,[5] W.A. Wenzel,[6] R.J. Wilson,[8] G. Wormser,[4] Ch. Yéche,[2] S. Yellin,[7] M. Zito.[2]

[1]Stanford Linear Accelerator Center, Stanford, CA 94309, USA.
[2]CEA, DAPNIA, CE-Saclay, F-91191, Gif-sur-Yvette Cedex, France.
[3]LPNHE des Universités Paris 6 et Paris 7, Tour 33, Bc 200, 4 Place Jussieu, F-75252, Paris, Cedex 05, France.
[4]LAL Orsay, Universite Paris Sud, Batiment 200, F-91405 Orsay Cedex, France.
[5]LPNHE de l'Ecole Polytechnique, Route de Saclay, F-91128 Palaiseau Cedex, France.
[6]Lawrence Berkeley National Laboratory, One Cyclotron Road, Berkeley, CA 94720, USA.
[7]Dept. of Physics, University of California, Santa Barbara, CA 93106, USA.
[8]Dept. of Physics, Colorado State University, Fort Collins, CO 80523, USA.
[9]Dept. of Physics, University of Cincinnati, Cincinnati, OH 45221, USA.

talk presented by S. Spanier[1] at

2000 IEEE
Nuclear Science Symposium
and
Medical Imaging Conference
Lyon, France
15 – 20 October, 2000

*Work supported by Department of Energy contract DE–AC03–76SF00515 (SLAC), DE-AC03-76SF00098 (LBNL), DE-AM03-76SF0010 (UCSB), and DE-FG03-93ER40788 (CSU) and PHY-95-11999 (Cincinnati).

Abstract

The DIRC (acronym for **D**etection of **I**nternally **R**eflected **C**herenkov (light)) is the ring imaging Cherenkov detector of the BABAR detector at the Pep-II ring of SLAC. It provides the identification of pions, kaons and protons for momenta up to 4 GeV/c with high efficiency. This is needed to reconstruct CP-violating B-decay final states and to provide B-meson flavour tagging for time dependent asymmetry measurements. The DIRC radiators consists of long rectangular bars made of synthetic fused silica and the photon detector is a water tank equipped with an array of 10,752 conventional photomultipliers. At the end of the year 2000 BABAR has recorded about 22 million $\bar{B}B$ pairs reaching the design luminosity of $\mathcal{L} = 3 \cdot 10^{33}/\mathrm{cm}^2\mathrm{s}$. The ability to keep the beam background level low at highest collision rates and the long term reliability of the DIRC components during continuous data taking are requirements of BABAR to accomplish its physics program.

1 Introduction

The physics program of the BABAR [1] detector is to observe CP violation and to probe the Standard Model of particle physics by collecting enough B-meson decay channels to overconstrain predictions. The source of B mesons is the PEP-II asymmetric e^+e^- collider, with beam energies of 9 GeV electrons upon 3.1 GeV positrons [2], which annihilate into $\Upsilon(4S)$ resonances with a resulting boost of $\gamma\beta \simeq 0.56$. The $\Upsilon(4S)$ resonance decays nearly exclusively in a pair of B and anti-B mesons. This allows precise measurements of time dependent asymmetries in B meson decays which can be related to the CP violating phase in the Cabbibo-Kobayashi-Maskawa matrix [3]. BABAR is a typical collider detector but asymmetrically placed around the interaction point to ensure nearly full solid angle coverage in boost (forward) direction, too. With the design luminosity of $3 \cdot 10^{33}/\mathrm{cm}^2\mathrm{s}$, reached at the end of year 2000, the production rate of B and anti-B meson pairs is 3 Hz.

In the BABAR experiment the separation of pions from kaons for particle momenta as high as 4 GeV/c in exclusive B-decays is essential. Only then one can distinguish, e.g., the channels $B^0 \to \pi^+\pi^-$ from $B^0 \to K^+\pi^-$ or $B^\pm \to \phi\pi^\pm$ from $B^\pm \to \phi K^\pm$, interesting for the measurement of indirect or direct CP violation. In fused silica (quartz), the Cherenkov threshold for kaons is $p = 460$ MeV/c. Up to a momentum of 700 MeV/c, the BABAR drift chamber can provide complementary information based on the dE/dx measurement. The difference in the Cherenkov angle between a pion and a kaon at $p = 4.0$ GeV/c is 6.5 mrad (the same difference occurs between a muon and a pion at 700 MeV/c). Therefore, 3σ π/K separation requires resolutions on the Cherenkov angle for a track of 2.2 mrad or better. Moreover, the flavour content of the recoil $B(\bar{B})$ needs to be tagged by identifying kaons in its successive decays. In addition, τ and charm spectroscopy profit from kaon identification.

The location of the particle identification system is radially between the drift chamber and the CsI(Tl) crystal calorimeter of BABAR. Therefore, a small radiation length is preferred to avoid deterioration of the excellent energy resolution of the calorimeter. This minimizes the radial dimension also, and keeps the amount of required calorimeter material (cost) small. Finally, to operate successfully in the high-luminosity environment of PEP-II, the Cherenkov detector has to be radiation hard, fast and tolerant of background.

The new type of detector for particle identification DIRC [4] covers the barrel region of the BABAR detector. It is a Cherenkov ring imaging device which utilizes totally internally reflecting Cherenkov photons in the visible and near UV range [5]. This technique reduces space requirements and increases the particle identification performance as compared to ring imaging detectors of the previous generation.

2 The Principle of the DIRC

The DIRC uses thin, long rectangular bars made of synthetic fused silica (quartz) [6] (H $\times$ W $\times$ L = 17 mm $\times$ 35 mm $\times$ 4900 mm) both as Cherenkov radiators and light guides (refractive index $n_1 \approx 1.47$). Bars are glued together from four pieces, each 1225 mm long. All together, 144 bars are arranged in a 12-sided polygonal barrel with a radius of about 84 cm around the beam axis. The DIRC bars extent 178 cm forward from the inter-

action point of BABAR covering 87% of the polar solid angle in the center-of-mass frame. The azimuthal coverage is 93% , since there are gaps between the bars at the 12 sides of the radiator polygon. Each 12 bars are housed in a bar box surrounded by nitrogen at NTP (index $n_2 \approx 1$). The assembly of the detector is shown in Fig. 1. The radiation length of bars is $X_0 = 14\%$, $X_0 = 19\%$ for the full assembly.

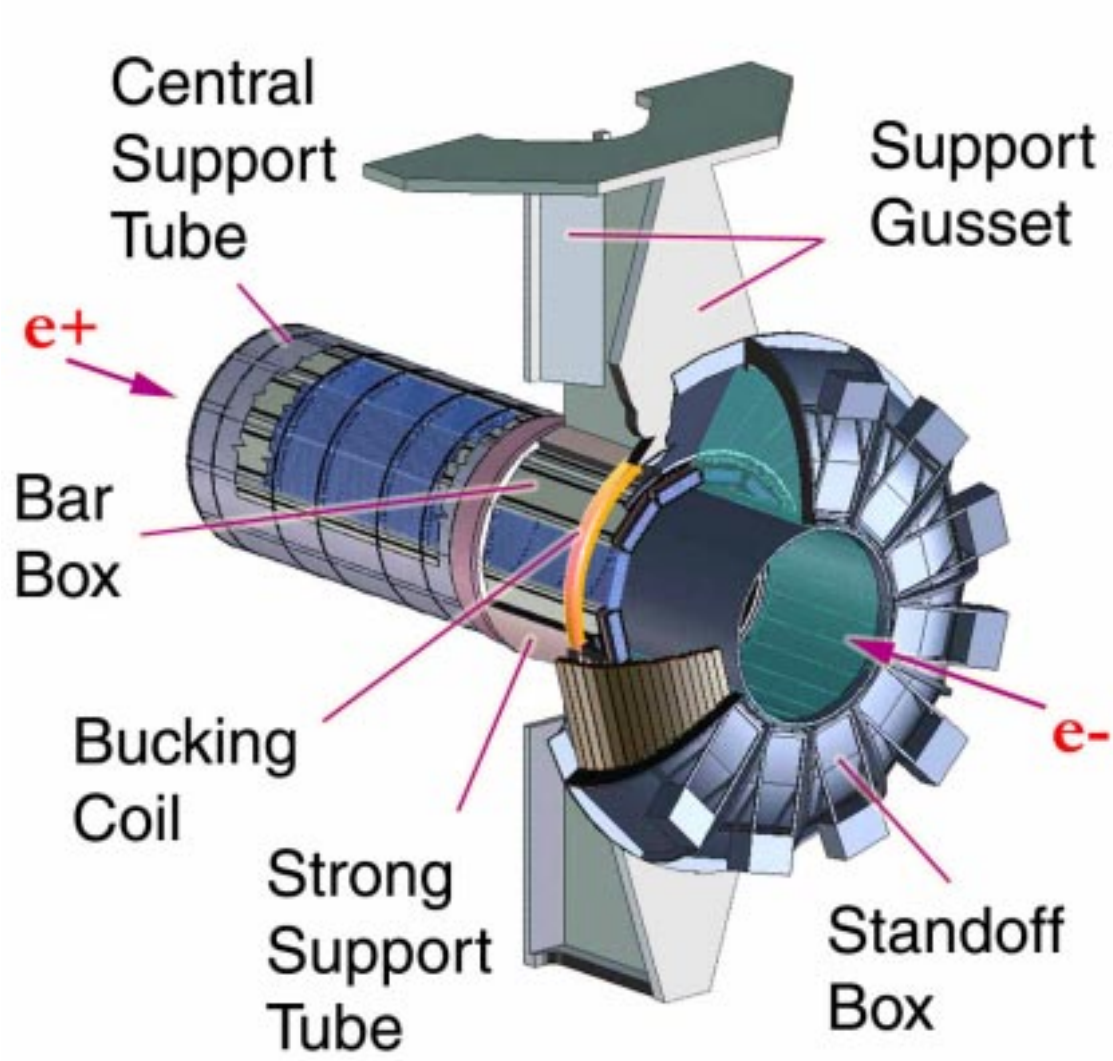

Figure 1: Schematical view of the DIRC assembly within BABAR.

Since the refractive index of the radiator bar n_1 is larger than $\sqrt{2}$, a certain fraction of the Cherenkov photons produced by a relativistic charged particle traversing the quartz bar will be totally internally reflected, regardless of the incidence angle of the tracks, and propagate along the length of the bar. Only one side is instrumented and a mirror (reflectivity $\approx$ 92%) is placed perpendicular to the bar axis on the other end, where positrons enter the BABAR detector. Due to the boost of the $\Upsilon(4S)$ the density of charged tracks is enhanced on

this side and hence it is less preferrable for the readout. Since a bar is made of high optical precision (mean surface reflectivity $\approx 99.96\%$ per bounce at 442 nm photon wavelength), the initial direction of the photon is captured within the rectangular bar during its propagation, modulo left/right, up/down and forward/backward ambiguities. The latter is resolved by the measurement of the photon arrival time.

Photons exiting the bar in downward direction, or with large angles in radial direction, are partly recovered into the instrumented area by a prism at the readout end. This optical element is 91 mm long and the top side has a 30^o opening angle. The bottom side is slightly tilted upwards by 6 mrad. It reduces the required photon-sensitive area by more than a factor of two.

A thin (9 mm) quartz window separates the prism from the so called standoff box (SOB), a water tank filled with 6000 liters of purified water (index $n_3 \approx 1.33$) in a toroidal shape (see Fig. 1. The backplane of the SOB is divided into 12 sectors, each equipped with 896 conventional phototubes [7] ($\approx 25\%$ detection efficiency at 400 nm wavelength, spectral range: 250 nm – 650 nm), pointing to the exit of a corresponding bar box. Hexagonal reflectors (light catchers) with water-resistant Rhodium surfaces surround the PMT cathodes improving the detection efficiency by about 20%. The ratio of refractive indices n_1/n_3 is nearly wavelength independent. It reduces internal reflection at the readout side of the bar. Furthermore, the exit angle is magnified by this ratio, increasing the position resolution of the photons.

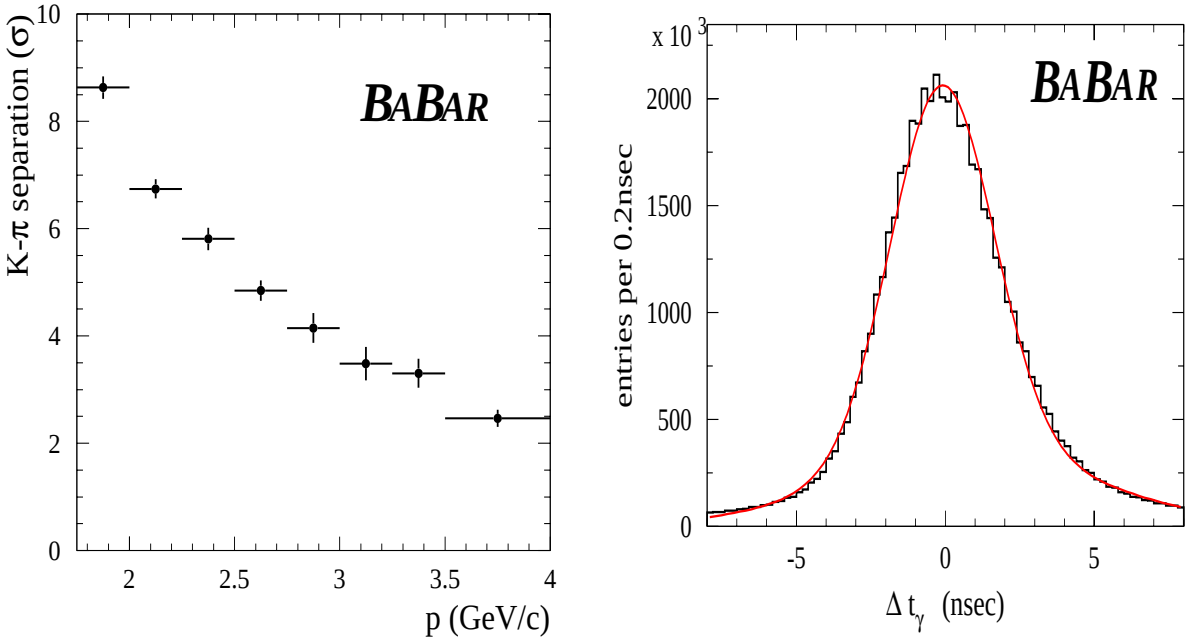

Figure 2: Left: Separation of pions and kaons in terms of Cherenkov angle resolution measured from the decay chain $D^{*+} \to D^0\pi_S^+$; $D^0 \to K^-\pi^+$ (and charge conjugated). Right: The distribution of the arrival time difference for Cherenkov photons after all corrections. The width is $\sigma = 1.7$ ns.

The detector provides a three dimensional measurement of the photon in the variables (α_x, α_y), the photon exit angles with respect to the bar axis and the hit time $t_{\rm hit}$ of the photon. The known spatial position of the bar through which the track passed and the phototube hit within a certain readout time interval is used to reconstruct the photon vector pointing from the center of the bar end to the center of the tube. This vector is then extrapolated back into the quartz bar using Snell's law, where the exit angles (ϕ_C, θ_c) with respect to the track are calculated. Most of the photon phase space $(\alpha_x, \alpha_y, t_{\rm hit})$ is mapped onto the Cherenkov angles (ϕ_C, θ_c) up to an average ambiguity of less than 3. The contribution of the timing apart from the resolution of the forward-backward propagating photons is not competitive with the position information, but it is crucial for suppression of beam background. Therefore, we discuss the measurement of the time in more detail in the next section. The Fig. 2 (left) shows the separation achieved for different momentum intervals measured with the decay $D^{*+} \to D^0\pi_S^+$; $D^0 \to K^-\pi^+$ (and charge conjugated), where the slow pion π_S^+ tags the charge of the pion from the D^0 decay. In this sample kaons are identified kinematically requiring a tight window around the $D^{*+} - D^0$ mass difference.

3 Timing

An important observable for a Cherenkov photon in the DIRC is the difference between its measured, t_m, and expected, t_e, arrival time, Δt. The measured arrival time t_m is obtained in several steps:

Bunch crossings in the Pep-II ring occur with a minimum spacing of 4.2 ns, while relevant physics is accepted at a rate of about 2 kHz. In the level-one (L1) trigger the bunch-crossing time is derived by fast pattern recognition in the superlayers of the drift chamber with a precision of about 70 ns (time jitter). This compares to the 50 ns width of the time distribution of Cherenkov photons created by tracks of a typical collision event in the quartz bars. To collect all photons of an event the readout interval in the DIRC is set to $\pm$300 ns with respect to the L1-trigger time.

The DIRC time, $t_{\rm hit}$, measurement is provided by a custom made digital chip TDC [8] which resides in the front-end boards mounted on the standoff box. The digitization clock is obtained by subdividing the 59.5 MHz BABAR system clock into 5 bits resulting in 0.525 ns wide time bins. It was chosen as a function of the 1.4 ± 0.2 ns phototube resolution. The time value is buffered for up to 12 μs, the latency of the L1-trigger. The hit time information is transferred by a 1.2 Gbit/s optical fiber from the front-end electronics of the twelve sectors pairwise into six readout modules (ROMs). After feature extraction it is provided to the event builder of BABAR.

At the level of reconstruction, corrections t_c for different delays in the readout electronics and phototube response time variations are applied. These are determined with a light pulser system which generates 1 ns pulse duration from a blue light LED, inserted by an optical fiber into 12 diffusers which are located above each bar box window facing the phototubes. The pulser produces roughly 10% photoelectron occupancy almost uniformly throughout the phototube array. The pulser is run at about 2 kHz to collect approximately 65000 light pulses for the determination of the mean-time delay of each tube with a statistical uncertainty of

better than 0.1 ns. The time delay values per channel are typically stable to a rms of less than 0.1 ns over more than one year of daily calibrations.

A measure of the bunch-crossing time, t_b, comes from a combined fit to drift-chamber tracks. Therefore, the resolution of t_b depends on the track multiplicity and angular distributions. Its typical resolution is about 2.5 ns.

Finally, the measured time is:

$$t_m = t_{\rm hit} - t_{\rm trigger} - t_c - t_b - t_{\rm offset}\,, \tag{1}$$

where $t_{\rm offset}$ is a global time offset. The precision in the parameter t_m for a Cherenkov photon is dominated by the bunch-crossing time t_b. Cherenkov photons originating from charged tracks in a collision event cluster in the arrival time as measured independently by the DIRC. The mean arrival time of the Cherenkov photons in an event, $< \delta t >_{\rm event}$, has a resolution of 100 - 200 ps. In practice, this self-triggering feature of the DIRC corrects the uncertainty in the bunch-crossing time (neglecting systematic corrections from detector alignment, trigger jitters or calibration). Furthermore, the mean value of the $< \delta t >_{\rm event}$ for a given run measures the deviation from $t_{\rm offset}$.

The expected arrival time, t_e, of the Cherenkov photon is a sum of the time-of-flight of the charged track from its origin to the quartz bar (typically 2-3 ns), the photon propagation time in the quartz bar and the prism along its reconstructed path and the travelling time through the water before reaching the surface of the photomultiplier.

Applying $< \delta t >_{\rm event}$ as correction yields a precision of better than 1.7 ns in $\Delta t = t_m - t_e$ - $< \delta t >_{\rm event}$ which is close to the intrinsic time resolution of the phototubes (see Fig. 2 (right)).

In principle, the resolution of the bunch-crossing time t_b becomes infinitesimal small if one can point out the occurence of the bunch in the Pep-II fill pattern which collided. The minimum bunch spacing of 4.2 ns is driven by the overall 476 MHz system clock Pep-II and BABAR are connected to. Current patterns consist of varying spacing of 12.8 ns, 8.4 ns or alternating 8.4 ns/4.2 ns. Therefore, the colliding bunches are found from a fit of the bunch pattern to the event Δt.

4 Background

Interactions of lost beam particles with rest gas in the beam pipe (Bremsstrahlung, Coulomb scattering) produce low energy photons (energy between 2 MeV and 2.5 MeV for 90% of them) which penetrate the water in the standoff box and the quartz bars. Those photons can generate secondary Cherenkov photons due to electrons from Coulomb scattering. Another source of secondary Cherenkov light are so called hot spots created in the complicated beam guidance near the interaction point by lost beam particles. They preferrentially hit beam pipe elements and produce secondaries which can enter the standoff box.

For a maximum background photon hit rate per phototube of 200 kHz one expects 1300 hits in a $\pm$300 ns readout time window corresponding to 12% occupancy. The readout efficiency rapidly degrades when counting rates exceed this threshold. The TDC and readout

electronics deadtime reaches several percent at 300 kHz and 20% at 700 kHz single tube hit rate. At the highest luminosity of $\mathcal{L} = 3 \cdot 10^{33}/cm^2 s$ the rate of single photon hits per tube is kept below 200 kHz. Therefore, fast feedback to the Pep-II control was provided by an analog signal from a tube in the innermost row of each standoff-box sector. Locations of hot spots are traced with CsI-crystal detectors placed along the beampipe and then covered with local lead shielding. To improve the DIRC data acquisition robustness an upgrade of the TDC which keeps the deadtime at a few percent for rates up to 1 MHz is scheduled for the year 2002. In addition, an cylindrical lead shielding in the inner radius of the standoff box is inserted for the year 2001 run.

On the other hand, in a time interval of ± 8 ns about 11 randomly distributed photons are present while for a typical multihadron event with 8 charged tracks entering the quartz bars at the same time all 240 signal photons are recorded. This demonstrates the potential of the time observable Δt in suppressing background at the reconstruction level. In Fig. 3 the effect is shown for a di-muon event.

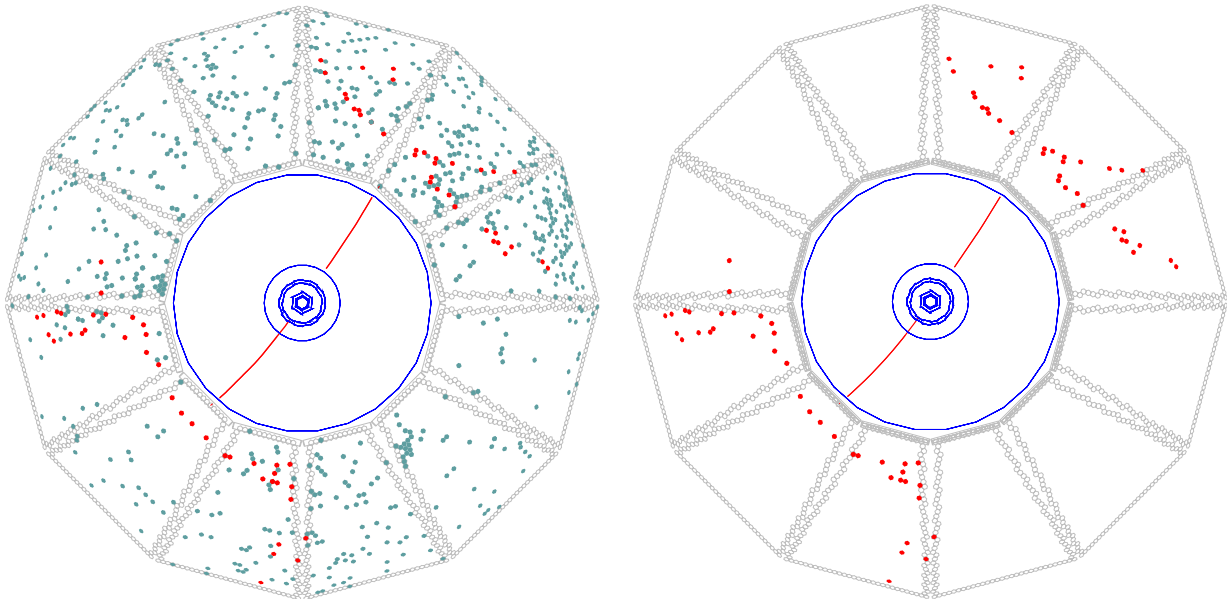

Figure 3: A typical $e^+e^- \to \mu^+\mu^-$ event in the $r\phi$ projection of the standoff box. Left: Photomultipliers which detect light within a time interval of ± 300 ns centered at the beam crossing time are shown as dots. Right: Only those phototubes are plotted which were hit within 8 ns of the expected Cherenkov photon arrival time.

5 Particle Identification

Particle identification uses a likelihood ratios based on the number of detected photons and the measured Cherenkov angles. The N photons associated with a charged track within 5σ intervals of the Cherenkov angle θ_C ($\sigma(\theta_C) = 10.2$ mr) and the time Δt ($\sigma(\Delta t) = 1.7$ ns) are

subjected to an unbinned maximum likelihood fit. The likelihood is shematically given by:

$$\mathcal{L} = \Pi\ (1-r)\, G(\phi_C, \theta_C) \cdot G(\Delta t) + r\, B \qquad , \tag{2}$$

allowing for remaining ambiguities in the photon solutions. Free parameters are the mean Cherenkov angle $< \theta_C >$ and the ratio of background to signal photons, r. The center of the reconstructed Cherenkov ring can be varied freely with the circle coordinate definition: $x_C =< \theta_C > \cos\phi_C$ and $x_C =< \theta_C > \sin\phi_C$. The probability density function for the Cherenkov angle and the time is a sum of two gaussians, where the smaller one represents the expected resolution and the second one parametrizes a broad background. The ratio between the two functions is prefixed to typically 10:1. The unbiased startvalue for $< \theta_C >$ is the expected Cherenkov angle from one of the particles e, μ, π, K, p which yields the highest likelihood.

The fitted Cherenkov angle $< \theta_C >$ and the number of signal and background photons for a charged track are translated into a likelihood l_i for the different particle hypotheses i. The first factor is a Gaussian g_i, with the expected Cherenkov angle Θ_i as mean value:

$$g_i = \frac{1}{\sqrt{2\pi}\sigma(< \theta_C >)} e^{-0.5\cdot\chi_i^2} \quad , \tag{3}$$

with

$$\chi_i = \frac{< \theta_C > -\Theta_i}{\sigma(< \theta_C >)} \quad , \qquad i = e, \mu, \pi, K, p\,. \tag{4}$$

To obtain a probability for all momenta one has to distinguish between above and below Cherenkov threshold. With t being the heaviest particle above the threshold, all particles heavier than t will have a constant probability of 0.2. This is the probability for each of the five candidates, if all of are below threshold. The normalization is defined in the following way:

$$\sum_{i=t+1}^{p} g_i \;=\; (p-t)\cdot 0.2 = m \tag{5}$$

$$\sum_{i=1}^{t} \;=\; 1-m \quad . \tag{6}$$

The second factor of the likelihood is based on photon counting: Signal photons $N_s = (1-r)N_a$, background photons $N_b = rN_a$ and expected number of photons $N_{exp,i}$ for particle hypothesis i as provided by a lookup table. The Poisson probabilities p_i are calculated the following:

$$p_i \;=\; \text{Poisson}(N_s + N_b, N_{exp,i} + N_b), \tag{7}$$

$$\sum_{i=e}^{p} p_i \;=\; 1 \quad , \qquad i = e, .., p. \tag{8}$$

Both probabilities are normalized independently. The total probability l_i is the product:

$$l_i = g_i \cdot p_i / \sum_{i=e}^{p} g_i \cdot p_i \qquad . \tag{9}$$

The particle hypothesis i is assigned to a charged track, if l_i is the highest likelihood. In particular kaons can be identified by the requirement

$$l_K > \alpha \cdot l_\pi \quad \text{and} \quad l_K > \beta \cdot l_p \tag{10}$$

with a certain choice of the likelihood ratios α and β tuned for example to achieve a certain kaon identification efficiency and purity. Figure 4 demonstrates the application of the DIRC for a sample selection based on the likelihood ratios $\alpha = \beta = 1$.

The efficiency for identifying correctly a charged kaon that hit a radiator bar and the probability to wrongly identify a pion as kaon are determined using D^0 decays selected kinematically from inclusive D^* production and are shown as a function of the track momentum in Fig. 5 for the same criterion Eq. 10 ($\alpha = \beta = 1$). The mean kaon selection efficiency and pion mis-identification are $96.2 \pm 0.2\%$ (stat.) and $2.1 \pm 0.1\%$ (stat.), respectively.

6 Operational Issues

After about 2 years of running, about 99.7% of all phototubes and electronic channels are still operating at nominal performance.

Corrosion of the PMT glass face plates that are immersed in the pure water of the standoff box has been observed. For most of the tubes, the observable effect is typically a slight cloudiness, but for ~ 50 of the tubes, it is much more pronounced. Extensive R&D has demonstrated that the corrosion is associated with a loss of sodium and boron from the surface of the glass. For most tubes, the corrosion rate is a few microns per year, and is expected to be acceptable for the full projected 10 year lifetime of the experiment. However, for the ~ 50 tubes, the wrong glass was used by the PMT manufacturer. This glass did not contain zinc, which makes it much more susceptible to rapid leaching. This leaching may eventually lead to either a loss of performance, or some risk of mechanical failure of the face plates, for these tubes. Direct measurements of the number of Cherenkov photons observed in di-muon events as a function of time suggest that the total loss of photons from all sources is less than 2%/year, although the accuracy of this number is limited by a number of systematic effects at this time.

7 Summary

The DIRC is a new type of Cherenkov detector for particle identification at BABAR, which provides excellent π-K separation for particle momenta up to 4 GeV/c. It is a reliable instrument successfully operated for two years.

8 Acknowledgments

This research is supported by the Department of Energy under contracts DE-AC03-76SF00515 (SLAC), DE-AC03-76SF00098 (LBNL), DE-AM03-76SF0010 (UCSB), and DE-FG03-93ER40788 (CSU); the National Science Foundation grant PHY-95-11999 (Cincinnati).

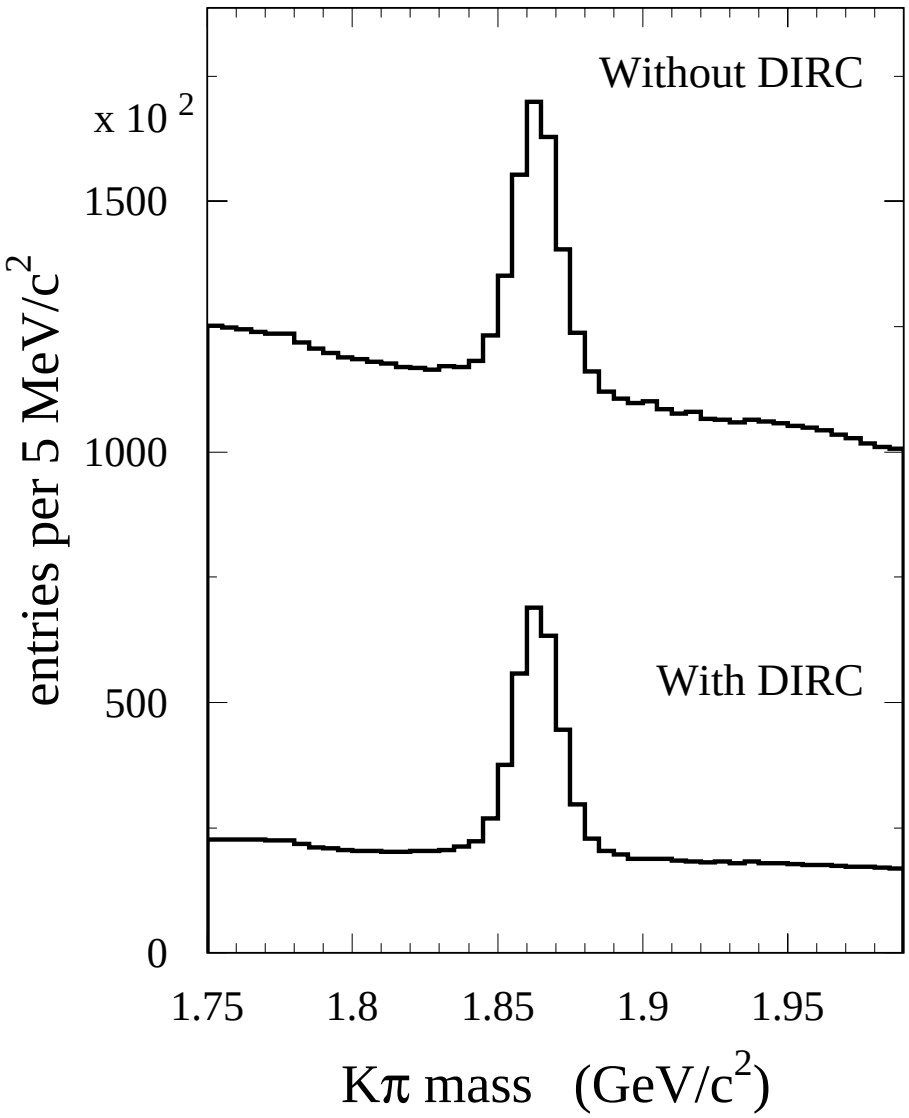

Figure 4: The invariant $K\pi$ mass spectra are shown without and with the use of the DIRC for kaon identification. The mass peak corresponds to the decay of the D^0 particle.

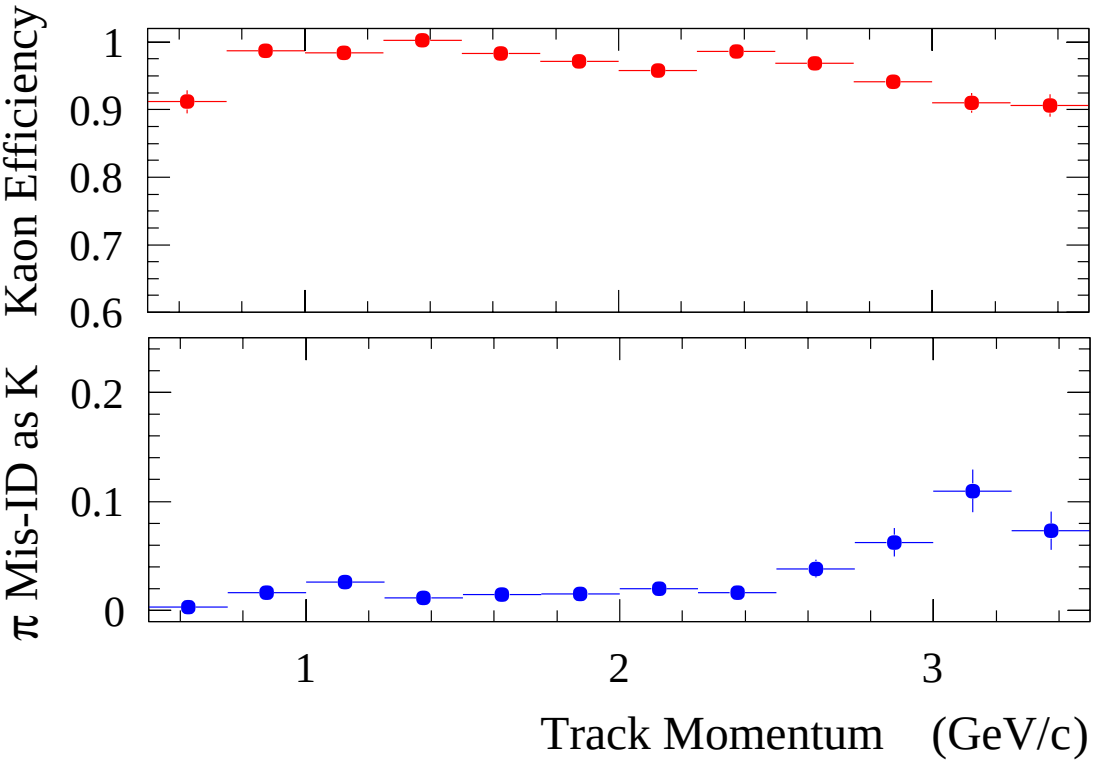

Figure 5: Efficiency and mis-identification probability for the selection of charged kaons from D^0 decays selected kinematically from inclusive D^* production as a function of track momentum.

References

[1] The BaBar Detector at the PEP-II B Factory, B. Aubert et al., SLAC PUB-8569, to be submitted to NIM

[2] J.T. Seeman, "Status of the PEP-II B Factory", talk given at the 14th Advanced ICFA Beam Dynamics Workshop: Beam Dynamics Issues for e^+e^- Factories (ICFA 97), Frascati, Italy, 1997; E. Bloom et al., "The PEP-II Asymmetric B Factory: Design Details and R&D Results", SLAC-PUB-6564 (1994); PEP-II: An Asymmetric B Factory. Conceptual Design Report, SLAC-R-418 (1993).

[3] The BaBar Collaboration, "The BaBar Physics Book", SLAC Report 504 (1998).

[4] B. Ratcliff, SLAC-PUB-5946 (1992), SLAC-PUB-6047 (1993);
P. Coyle et al., Nucl. Inst. Methods A343, 292 (1994).

[5] The BaBar DIRC Collaboration, I. Adam et al.,
IEEE Trans. Nucl. Sci. 45 (1998) 450, 657
J. Cohen-Tanugi, M. C. Convery, B. N. Ratcliff, X. Sarazin, J. Schwiening, J. Va'vra, SLAC-JOURNAL-ICFA-21, *ICFA Instrumentation Bulletin,* Fall 2000 Issue.

[6] The provider of fused silica: TSL Group PCL,
P.O. Box 6, Wallsend, Tyne & Wear, NE28 6DG, England.
Quartz Products Co., 1600 W. Lee St., Louisville, Kentucky 40201.
Manufacturer of quartz bars: Boeing, Rockedyne Division, 2511 C Broadbent Parkway NE, Albuquerque, New Mexico 87107.

[7] Manufacturer of phototubes: Electron Tubes Limited, (formerly: Thorn EMI Electron Tubes), Bury Street, Ruislip, Middlesex HA47TA, U.K.

[8] P. Bailly et al., Nucl. Inst. Methods A432, 157 (1999),
P. Bailly et al., Nucl. Inst. Methods A433, 450 (1999).